The effects of elastic scattering in neutral atom transport

D. N. Ruzic

Citation: Phys. Fluids B **5**, 3140 (1993); doi: 10.1063/1.860651
View online: http://dx.doi.org/10.1063/1.860651
View Table of Contents: http://pop.aip.org/resource/1/PFBPEI/v5/i9
Published by the American Institute of Physics.

The effects of elastic scattering in neutral atom transport

D. N. Ruzic
University of Illinois, 103 South Goodwin Avenue, Urbana Illinois 61801

(Received 14 December 1992; accepted 21 May 1993)

Neutral atom elastic collisions are one of the dominant interactions in the edge of a high recycling diverted plasma. Starting from the quantum interatomic potentials, the scattering functions are derived for H on H^+, H on H_2, and He on H_2 in the energy range of 0.1–1000 eV following classical scattering theory and an impact parameter formulation. Potentials for both the gerade and ungerade electronic wavefunctions were included. An algorithm for the addition of these reactions to the DEGAS [J. Comput. Phys. **46**, 309 (1982)] code is presented and used to simulate three test problems: (1) the transport of neutral atoms through a dilute edge plasma, (2) the penetration of neutral atoms into a dense plasma from a divertor plate, and (3) the transmittance of neutral atoms through a pump duct. In all three cases the inclusion of elastic scattering has a significant influence on the neutral atom density, temperature, and flux to the walls.

I. INTRODUCTION

The study of neutral atom transport has become more central to the success of magnetic fusion energy, as attention has turned to the issues of energy removal, material lifetimes, fueling, and exhaust. These issues must be addressed in the planning of the next generation of long-pulsed or steady-state diverted machines. In the divertor region neutral atoms are recycled many times. The flux amplification (the number of ions striking the plate compared to the net number of ions crossing the separatrix) may be on the order of 100. The neutral atoms are produced by the impact of ions on the divertor and by the dissociative electron-impact ionization of molecules desorbed from the surface. The atoms from dissociation at a few eV, and the reflected atoms with 10 eV to 100 eV will eventually charge exchange with fast ions or be ionized, completing the ion-to-neutral-to-ion cycle. Before this occurs the atoms may undergo elastic scattering with ions, atoms, or molecules. These collisions will change the energy and the trajectory of the neutrals altering the character of the recycling and a number of other important parameters.

One altered parameter is the plasma fueling. Ionization of neutral atoms form the source term for plasma generation. Penetration of neutral atoms through the scrape-off layer and into the core is the only mechanism for deuterium and tritium replacement. Scattering of fast neutrals effects the location of this source term. Fast atoms that do not become ionized strike the divertor plate, first wall, or limiter structures instead. These atoms may sputter the surfaces or become retained in the material.

Related to fueling is the removal of the helium ash produced from the fusion reactions. In a device where the plasma burn time is longer than the particle confinement time, recycling is responsible for maintaining the fuel density, and helium must be exhausted at the same rate it is produced. When the plasma burn length is also greater than the pumping constant for the device, the neutral transport is essential for the removal of all the gases. In a long-pulsed or steady-state machine, wall conditioning, to create a massive sorption pump out of the walls, is not an option. The design of the ducts and pumps become critical to the ability to maintain the desired steady-state pressure and fuel/ash ratio.

In all these cases: recycling, plasma fueling, tritium retention, helium removal, pumping speed, and divertor/pump duct geometry; a detailed understanding of the transport of neutral atoms may be important. As this paper shows, one of the largest cross sections for ion–neutral and neutral–neutral interactions is elastic scattering. DEGAS[1] and most other neutral transport codes do not consider such reactions. Yet, the DEGAS neutral transport code is often used in such calculations, since it allows an arbitrary three-dimensional geometry, predicts *h*-alpha and charge exchange signals, and does include all the dissociation, charge exchange, ionization, and wall reactions in detail.

Understanding and incorporating elastic scattering into such a Monte Carlo transport code is complicated by an inherent difference between the two classes of collisions. In elastic scattering, the scattering angle is forward peaked, and both its angular dependence and its magnitude are a function of the relative energy between the two particles. Elastic collisions change the magnitude and direction of the velocity. The other types of collisions, as implemented by DEGAS, depend only on the locally defined properties of electron temperature, ion temperature, and density. An occurrence of an ionization or a dissociation only changes the weight of the particle, and not its velocity vector. The occurrence of a charge exchange creates a completely new neutral atom whose new direction is picked from the local ion-temperature Maxwellian.

In this paper the differential scattering cross section for ion–neutral and neutral–neutral interactions from the interatomic potentials is derived. Then an algorithm for the inclusions of such interactions in DEGAS is developed and implemented. Finally, three examples of the effects of the elastic scattering are shown: penetration of neutrals into a dilute plasma (transport from the divertor through the edge), penetration of neutrals into a dense plasma (fueling

 0899-8221/93/5(9)/3140/8/$6.00

of the plasma from the divertor plate), and penetration of neutrals through a cold molecular gas (transmittance through a pump duct and power loss in a gaseous divertor.

II. THEORY

A. Interatomic potentials

The three interactions that dominate the neutral elastic collisions in a magnetic fusion device have been analyzed in detail. These are H on H^+, H on H_2, and He on H_2. H atoms are always the minority species. For virtually every region of a magnetic fusion device, the density of ions or the density of molecules are higher than the density of atoms. Thus H–H collisions are a second-order effect. The deuterium isotope is simulated in the examples, but the methodology is valid for any of the hydrogenic species. A correction to other species is made through the reduced mass parameter, $\mu=(m_1m_2)/(m_1+m_2)$, where m_1 and m_2 are the masses of the scattering species. The interatomic potentials for the heavier isotopes are not expected to deviate significantly from those for H, and the potential for H on H^+ have been rigorously derived from first principle quantum mechanics.[2] The pair can form a bound state (H_2^+) if the electronic wavefunctions form in the singlet *s*, or gerade, configuration. The gerade state has a potential minimum of -3 eV occurring at a distance between the two nuclei of 0.95 A. There is a $\frac{1}{4}$ occurrence of this gerade wavefunction and a $\frac{3}{4}$ occurrence of a triplet-2*p* state, known as the ungerade wavefunction. This ungerade state will not form a bound state and its interatomic potential is repulsive at all distances.

In the H on H_2[3–5] and He on H_2[6,7] interactions, no bound state is possible, so the interaction is repulsive at all distances. The target, however, is not spherically symmetric. A different potential, and therefore a differing scattering cross section, results for each orientation of the collision vector and the line between the two nuclei in the molecule. Though some quantum mechanical calculations exist for the potential as a function of molecular orientation, all orientations share a portion of the potential treating the molecule as spherically symmetric. In this work only the repulsive spherically symmetric part of the potential was considered. The resultant scattering angles should be averaged over all the orientations instead, but little difference is expected in the results. The potentials for different orientations only differ at the very lowest energies. The greatest effect would be on particles with energies less than 1 eV.

B. Scattering cross sections

Classical scattering theory[2,8] is used to find the scattering angle given the initial energy, $E_{\rm lab}$ and the impact parameter, b. Let the interatomic potential be denoted by $V(r)$, where the origin is the center of the force, and a particle of reduced mass μ is incident at an impact parameter b. Figure 1 defines the trajectory coordinate system (r,φ). The distance of closest approach is r_0. The scattering angle, $\varphi(r=\infty)$, is $\theta_{\rm com}$. Conservation of energy leads to

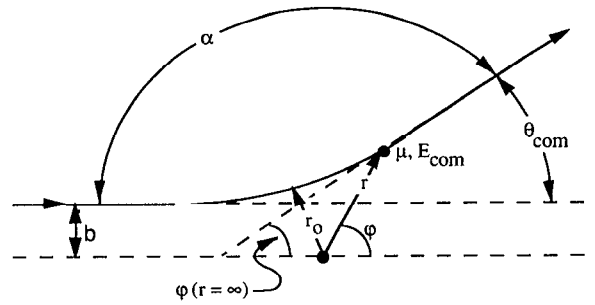

FIG. 1. Diagram of scattering coordinate system in the relative frame.

$$E_{\rm com}=V(r)+\tfrac{1}{2}\mu(r'^2+r^2\varphi'^2). \tag{1}$$

Conservation of angular momentum leads to

$$vb=r^2\varphi'. \tag{2}$$

Substituting Eq. (2) into Eq. (1), an equation for r', the derivative of r with respect to time, emerges:

$$r'=\left(\frac{2}{\mu}\left[E_{\rm com}-V(r)\right]-\frac{v^2b^2}{r^2}\right)^{1/2}. \tag{3}$$

Since $r'=0$ at the distance of closest approach that distance is constrained by the following condition:

$$b^2=r_0^2\left(1-\frac{V(r_0)}{E_{\rm com}}\right). \tag{4}$$

The equation of motion for the particle can be found by substituting (3) into (2):

$$\frac{d\varphi}{dr}=\frac{vb}{r^2}\left[\frac{2}{\mu}\left[E_{\rm com}-V(r)\right]-\frac{v^2b^2}{r^2}\right]^{1/2}. \tag{5}$$

To determine the scattering angle, Fig. 1 shows that $\pi=\alpha+\theta_{\rm com}$. Since $\alpha/2=[\varphi(r=\infty)-\varphi(r=r_0)]$, Eq. (5) can be integrated from r_0 to ∞ to yield

$$\theta_{\rm com}=\pi-2b\int_{r_0}^{\infty}\frac{dr}{r^2[1-V(r)/E_{\rm com}-b^2/r^2]^{1/2}}. \tag{6}$$

This integral is indefinite since the integrand equals infinity at $r=r_0$. This is one of the faults of the classical approach. The integral can be integrated from $r=r_0+\epsilon$ to $r=\infty$, where ϵ is a very small number. One can define $\Delta\varphi\equiv\varphi(r=r_0+\epsilon)-\varphi(r=r_0)$, then at $r=r_0+\epsilon$, $\alpha/2=[\varphi(r=\infty)-\varphi(r=r_0+\epsilon)+\Delta\varphi]$, and $\theta_{\rm com}=\pi-\Delta\varphi/2-\alpha/2$. Equation (6) becomes

$$\theta_{\rm com}=\pi-2\,\Delta\varphi -2b\int_{r_0+\epsilon}^{\infty}\frac{dr}{r^2[1-V(r)/E_{\rm com}-b^2/r^2]^{1/2}}. \tag{7}$$

As ϵ goes to 0, $\Delta\varphi=(d\varphi/dr)\epsilon$. Since ϵ is small, a linear interpolation can be used to evaluate $\Delta\varphi$. This is justified by true quantum mechanical calculations of scattering angles, where the differential scattering cross section reaches a finite value instead of going to infinity as theta goes to zero. Evaluating Eq. (5) at $r=r_0+\epsilon/2$ gives an approximate value for $\Delta\varphi$ of

TABLE I. The five fitting parameters for an Abrahmasson type potential given by Eq. (10) for each of the elastic scattering interactions considered in this work. For r in Å, these numbers yield $V(r)$ in eV.

Interaction	A	B	C	D	E
H on H^+, gerade	2000	6.8	1.67	1.55	6.45
H on H^+, ungerade	200	2.6	0.10	0.08	7.00
H on H_2, spherical	2420	6.0	0.547 28	0.40	8.00
He on H_2, spherical	1038	4.4	0.02	0.65	12.00

$$\Delta\varphi=\frac{\epsilon b}{(r_0+\epsilon/2)^2[1-V(r_0+\epsilon/2)/E_{\rm com}-b^2/(r_0+\epsilon/2)^2]^{1/2}}. \tag{8}$$

The other limit of integration in Eq. (7), $r=\infty$, only needs to be carried until $V(r)$ is so close to 0 that scattering from that potential magnitude leads to negligible scattering. Let that distance be called L. For $V(r)=0$, Eq. (7) can be solved analytically between L and infinity to yield $\theta_{\rm com}=\sin^{-1}(b/L)$. The entire scattering integral is finally given by

$$\theta_{\rm com}=\pi-2\left[\Delta\varphi+b\int_{r_0+\epsilon}^{L}\frac{dr}{r^2[1-V(r)/E_{\rm com}-b^2/r^2]^{1/2}}+\sin^{-1}\left(\frac{b}{L}\right)\right]. \tag{9}$$

Analytic fits were made to the four interaction potentials using an Abrahamson[9] type potential with an attractive well:

$$V(r)=Ae^{-Br}-\left(\frac{C}{r}\right)^6+\left(\frac{D}{r}\right)^E. \tag{10}$$

The five parameters (A, B, C, D, and E) for each of the four potentials are given in Table I. Though the shape of the attractive well of the gerade potential was not fit exactly by this function, the depth and location of the well's minimum is correct. Its location and magnitude had the largest effect on the resultant scattering angles. Some other aspects of each of the potentials are also deficient, but each of the potentials had realistic fits in the energy range of 1–100 eV. This is the most likely range for elastic scattering collisions in plasma devices and had the largest effect on the calculations.

To evaluate Eq. (9) once an impact parameter and an energy is chosen, Newton's method[10] is used to solve (4) for r_0, and then Simpson's rule[11] is used to integrate (9). The sensitivity to the results to the choice of ϵ or L is small. An ϵ of 10^{-4} and a L of 5 Å were generally used. The result was quite sensitive to the number of divisions used in the Simpson rule integration. As the number of divisions per Å increased, the scattering angles reached an asymptotic value. Most cases used 6000 divisions per Å. This ensured a less than 4% deviation from the asymptotic scattering angle.

C. Monte Carlo implementation

Though Eq. (9) could be evaluated for each scattering event, it is more effective to compute a lookup table of scattering angles as a function of impact parameter b in 0.05 Å increments, and as a function of energy from 0.1–50 eV in 0.1 eV increments, from 51 to 100 eV in 1 eV increments and 105–1000 eV in 5 eV increments. The entire range of impact parameters was not always calculated. The entries in the table were not computed once the scattering angle in the center-of-mass frame was less than 1° and the potential minimum, if existent, was passed. Such a lookup table was generated for each of the four interactions. The results for $\theta_{\rm com}$ as a function of b is shown in Figs. 2(a)–2(d).

Note that the energy dependence of the scattering angle is very marked. At high energies the scattering is extremely forward peaked. At low energies the rainbow phenomena—very large attractive scattering—becomes apparent. These are orbits that form a quasibound state and then fly off in virtually any direction. Such behavior also exists in quantum mechanical calculations, but interferences dominate in the rainbow region and the scattering angle rapidly rises and falls over a very small impact parameter range. Since the impact parameter is chosen in a Monte Carlo fashion anyway, no loss in generality comes from using the classical approach.

The DEGAS code employs pseudocollisions to track particles. The local mean-free path of a particle is calculated as the velocity of the neutral particle divided by the total reaction rate. The total reaction rate includes reaction rates for real collisions: charge exchange, ionization, and dissociation; and a user-specified fictitious reaction rate. After the particle is stepped, a random number is generated to determine if a real reaction occurred, or if the pseudocollision was fictitious. Fictitious reactions do not alter the velocity vector or probability weight of the particle, but they do allow a contribution to the density of particles in that cell to be summed. Real collisions alter the weight of the neutral particle for an ionization. They alter its velocity vector for a charge exchange. They alter the particles species type, weight, and velocity vector for a dissociation.

Since elastic scattering reactions only change the particles velocity vector and do not preclude it from undergoing the other reactions, the elastic scattering reactions were added to this algorithm as follows. Given the density of the interacting species, n, and the total cross section for the elastic interaction σ, the mean-free path for an elastic collision is λ, where

$$\lambda=1/(n\sigma). \tag{11}$$

Since the particle will be stepped λ_0 in DEGAS whether a real or a fictitious collision is logged, the probability of elastic collisions during that step is calculated. The probability of having no collisions in a step size λ_0 is p_0, and is given by

$$r_0=\exp(-\lambda_0/\lambda). \tag{12}$$

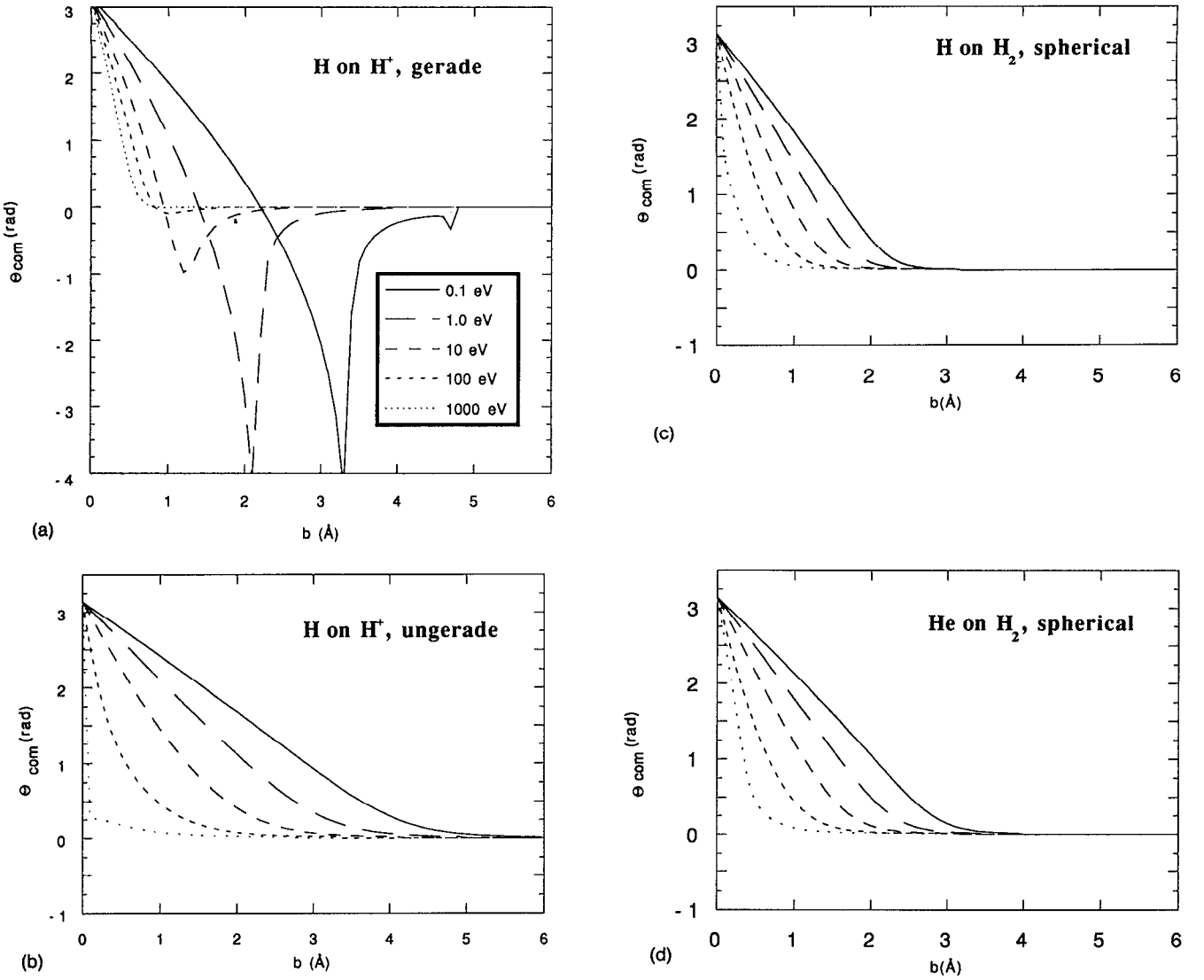

FIG. 2. Center-of-mass scattering angle versus impact parameter as a function of energy. Results from (a) H on H^+, gerade electronic wavefunction; (b) H on H^+, ungerade electronic wavefunction; (c) H on H_2, spherically symmetric potential; and (d) He on H_2, spherically symmetric potential, are shown.

The probability of having one or more elastic collisions during a step size λ_0 is $1-p_0$.

Figure 3(a) shows p_0 as a function of λ_0/λ. This figure is also helpful in showing how to calculate the probability of multiple collisions during the step of size λ_0. Given that one collision has occurred, the chance of having more collisions is calculated in two pieces. First, a random number, p_1 is picked between 1 and p_0. The "actual" step size for the first collision, λ_1, is then given by

$$\lambda_1 = -\lambda \ln(p_1). \tag{13}$$

Now the probability of having a collision in a step size of $\lambda_0-\lambda_1$ is calculated. Instead of $1-\exp(-\lambda_0/\lambda)$, it is

$$1-e^{-(\lambda_0-\lambda_1)/\lambda}=1-p_0/p_1. \tag{14}$$

This procedure is continued. Given two collisions the chance for a third is $1-p_0/(p_1p_2)$, etc.

Figure 3(b) shows the interpretation of the particles flight path. The effects of the scatterings are summed and the particle is placed at the end of the original step with a new velocity. Since λ_0 is a user-adjustable quantity by altering the fictitious reaction rate in each cell, the average number of collisions per step can be limited to approximately e^{-1}. By choosing a fictitious reaction rate that approximates the elastic collision rate, the validity of the pseudocollision algorithm is preserved, and the difficulty of adding a rate based on an energy-dependent cross section is avoided. There is some error introduced by this procedure in the position of the particle. However, since the scattering is extremely forward peaked for most energy and impact parameter combinations, the error in the particles' trajectory is small. Variations in the fictitious reaction rate over a wide range do not produce significant deviations in the results. There is no error in the attenuation of the particles since elastic scattering only changes the velocity and not the identity, weight, or existence of the particle being followed.

If a particle does elastically scatter and a real collision

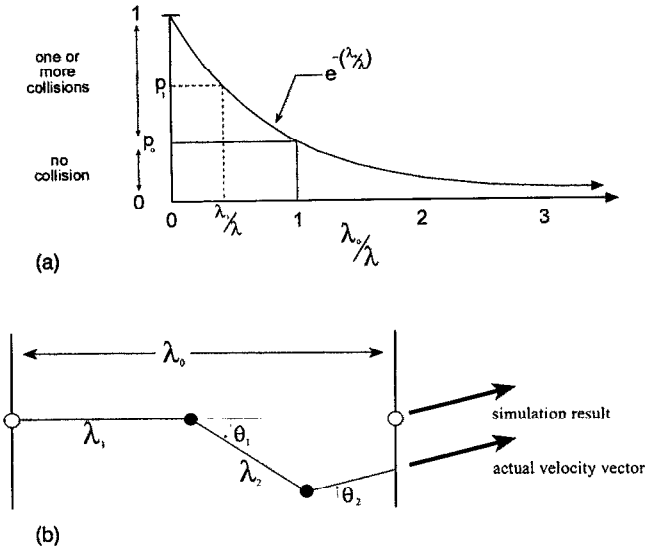

FIG. 3. (a) The elastic collision probability distribution within a step of size λ_0, given the mean-free path of the elastic collision, λ. (b) The tracking algorithm used in the simulation compared to the actual flight path.

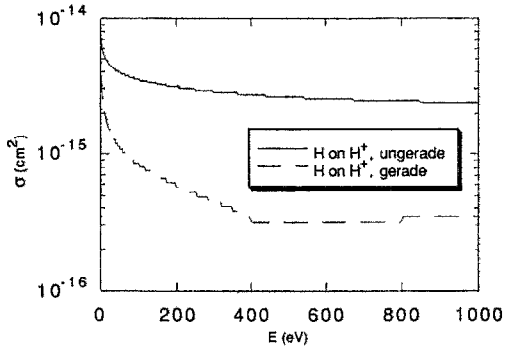

FIG. 4. The total scattering cross section for H on H^+ elastic collisions, resulting in scattering of greater than one degree in the center-of-mass frame.

is logged during the step, the neutral atoms velocity vector is changed first, and then the real collision is treated normally. The only exception is the rare rainbow collision in the atom–ion gerade function with identical particles. In this case the identity of the particle is lost during the orbiting interaction, and the probability for charge exchange is set to 0.50 after the elastic event and before the occurrence of a real charge exchange collision is determined.

In an elastic scattering collision, a collision partner must be chosen. A partner cannot simply be chosen from the local Maxwellian distribution of ions or molecules since the energy dependence of the total elastic scattering cross section is based on the relative velocity of the two particles. A rejection technique must be applied, comparing the candidate partners with the true value of $\sigma(E)$ for that particular pairing. Flow velocities are added to the potential scattering candidates as a function of position in the lab frame before a partner is selected. The lab frame velocities of both the particle and its partner have to be converted to the center of mass and then to the relative coordinate system before the scattering angle can be found.

Once the collision partner is chosen and the coordinates transformed, the scattering angle for each elastic scattering collision is calculated by choosing an impact parameter b from $b=\mathrm{sqrt}(r_1)b_{\max}$, where r_1 is a random number between 0 and 1 and $b_{\max}$ is the maximum value of b to cause at least 1° of scattering. The total scattering cross section for scattering greater than 1° is $\sigma=\pi b_{\max}^2$. With this formalism, and known scattering functions $\theta=\theta(b,E)$, a $b_{\max}$ could be chosen arbitrarily large. The particular value of $\sigma(E)$ for the elastic scattering events only influences the calculation time, not the results, since $\sigma(E)$ determines λ. Figure 4 shows the total scattering cross sections used in this work. The neutral–ion interactions initially drop off with energy because the cross section is chosen to represent the chance of scattering greater than one degree at all energies.

For simplicity the neutral atom–molecule collisions were treated in a modified manner. Since the velocity distribution of the molecules is extremely narrow ($T=1/20$ eV vs tens of eV for the incoming atom) a rejection technique to choose a collision partner is not needed. In addition, the $b_{\max}$, and therefore the total cross section, does not need to be energy dependent. A $b_{\max}$ of 3.1 A was used for the H on H_2 interaction, and a $b_{\max}$ of 4.0 A was used for the He on H_2 interaction. The scattering itself is still energy dependent and comes from a θ lookup table calculated for all entries, not just those that yield greater than one degree scattering. At the lowest energy, 0.1 eV, any $b<b_{\max}$ will lead to scattering of greater than one degree. At high energies, most of the b's selected, except for very small values, will lead to no scattering at all—just as if a lower $b_{\max}$ had been employed.

In all cases the amount of scattering is independent of the fictitious reaction rate. The fictitious reaction rate only sets λ_0. The reaction rates are determined by the density in the cells and by the velocity-dependent cross section of the interaction in question. However, the H_2 density is an input to the code. In some cases the inclusion of elastic scattering may alter the neutral molecular density. This code is not self-consistent in this regard. However, in most applications the effect is not large[12] and can be treated by this algorithm in an iterative fashion.

III. RESULTS

A. Transport of neutrals in a dilute plasma

To test the effects of elastic scattering on neutral transport through a dilute plasma (such as one would find traversing the edge region of a fusion device between the edge of the divertor plate, first wall, or pump duct and the plasma), a three zone plasma was constructed. Figure 5 shows the 60 cm by 60 cm test volume and the plasma densities and temperatures. The neutral atoms were all started at one point and allowed to enter the plasma with the reflected energy of an 18 eV D^+ normally incident on C, and a cosine angular distribution. DEGAS follows and computes the three-dimensional velocity and position vec-

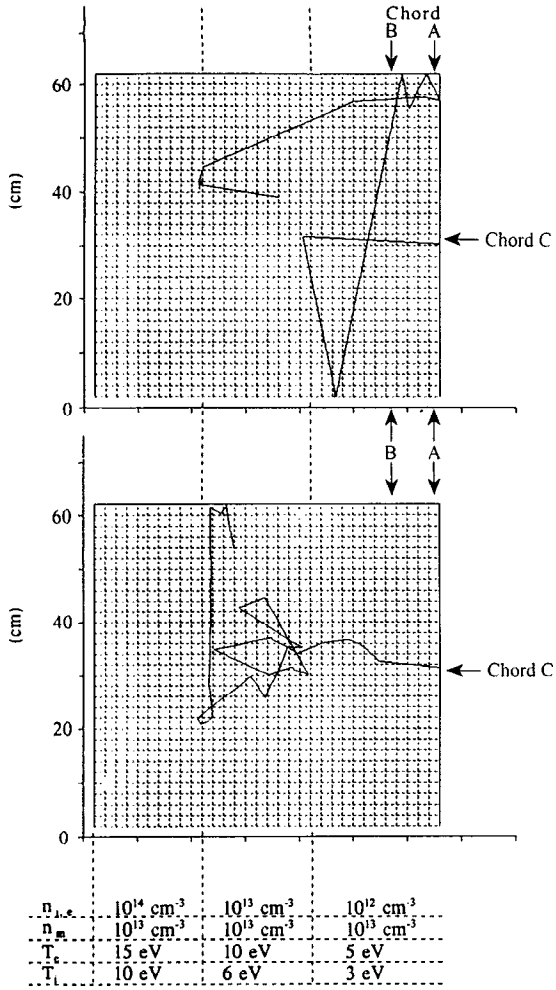

FIG. 5. Temperature and densities in a three-zone dilute-plasma model. Test flights are launched from the right-hand side. Two sample trajectories are shown: (top) no elastic collisions, and (bottom) with elastic collisions.

tors and then displays their projection onto the plane. The extent of the plasma is treated as infinite into and out of the plane.

Two test flights trajectories are superimposed on the simulation projection. Figure 5(top) shows a typical flight when elastic collisions are not included. The atom either charge exchanges, causing a large change in angle, or continues in a straight line until it strikes a wall. The weight of the particle steadily decreases as ionization event occur until the weight has fallen by a user-defined factor. In this simulation a minimum weight of 1×10^{-4} was used.

Figure 5(bottom) shows a typical test flight when elastic collisions are included. In the least dense region elastic collisions with molecules dominate and the scattering angle are very small. In the middle region both charge exchange and neutral–ion and neutral–molecule reactions occur leading to a mix of small angle scatterings and large angle charge exchange events. Finally, in the densest region, charge exchange and ionization dominate. For 1000 test flights into this geometry 4983 neutral atom–ion collisions occurred and 117 855 neutral atom–neutral molecule collisions occurred.

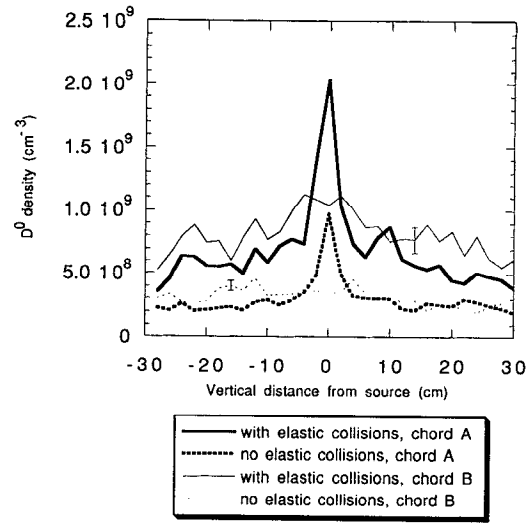

FIG. 6. Neutral density along chords A and B (shown in Fig. 5) for the case with elastic collisions and for no elastic collisions. Chord A is at the source plane; chord B is 10 cm away. The small peaks in the wings of the distribution are due to Monte Carlo statistical noise. Representative error bars are shown.

The effect on the distribution of neutral density in the plasma was significant. The inclusion of elastic collisions produced density contours expanding from the source. The distribution was reminiscent of one from diffusion. In the absence of elastic collisions the neutral density did not stay peaked but spread quickly in the vertical direction of Fig. 5. This is illustrated in Fig. 6. The neutral density is plotted along the vertical chords marked A and B in Fig. 5. Even though both cases had the same total current of neutrals sourced, the density is much larger in both chord A and B when elastic collision are included, because the neutrals do not spread as far from the source. The peaking in the center is clearly seen in both of these chords. For the case with no elastic collisions, the source is still seen in chord A, but dies out quickly. The profile is uniform 10 cm away in chord B.

The transport of neutral atoms along the central chord (marked C in figure 5) is plotted in Fig. 7. When elastic scattering is included the higher density along the center chord is clearly seen in the lowest ion density region. The mid-density region exhibits an exponential neutral density decay. The agreement between the neutral densities both with and without elastic collisions in this region may be merely coincidental since each had a differing density at the start of the region. In both cases very few neutrals survive to the densest region of the plasma.

B. Penetration into a dense plasma

To study the penetration of neutral atoms into a dense plasma, as one may find traveling along the field lines away from a divertor plate, another simulation was conducted. In this case plasma values were taken from a B2[13] simulation for a mid-sized high recycling diverted tokamak. The plasma values only varied as a function of distance away from the divertor plate. The density at the divertor plate

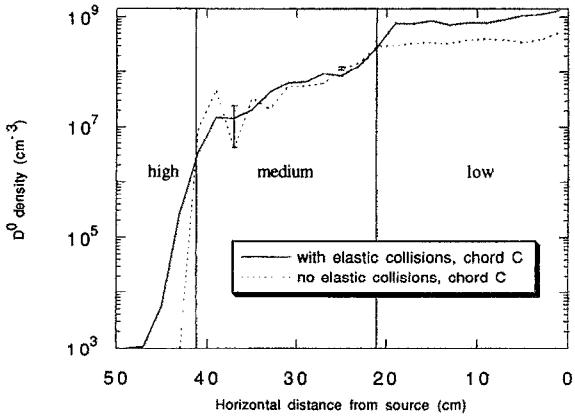

FIG. 7. Neutral density along chord C (shown in Fig. 5) for the case with elastic collisions and for no elastic collisions in the three-zone test plasma. The plasmas temperature and density are higher at the left and lower at the right. The statistical error in the data is on the order of the fluctuations seen in the data. Representative error bars are shown.

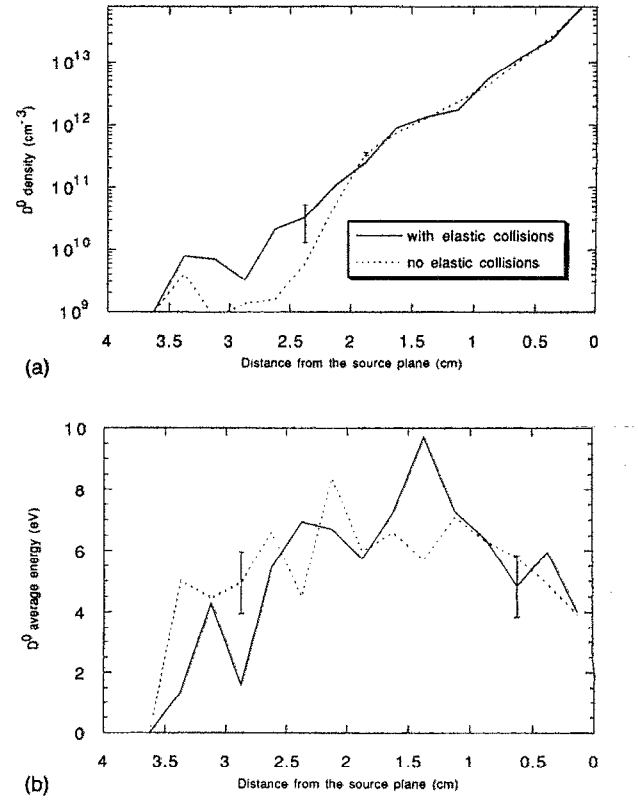

FIG. 8. Penetration of neutral atoms into a dense plasma at a divertor plate. (a) Neutral density and (b) neutral average energy as a function of distance from the source plane. The statistical error in the density is on the order of the fluctuations seen in the data. Representative error bars are shown.

was 2.2×10^{14} cm^{-3}. It gradually fell to 0.68×10^{13} cm^{-3}, 60 cm away. The electron temperature at the divertor plate was 12 eV, which climbed to 44 eV at a distance of 60 cm from the plate. Over this same distance the ion temperature rose from 6 eV at the plate to 46 eV. A large number of zones were placed very close to the divertor plate since most of the events occurred in the first few cm. The source was distributed across the entire plane and not concentrated at one point. The atoms and molecules were born from ions striking the divertor plate with $3T_e+T_i$ (42 eV). At this energy most of the neutrals came into the simulation as neutral molecules. For 1000 neutral flights, 2208 neutral–ion elastic collisions occurred. The neutral molecule density was set at zero.

Figure 8(a) shows an exponential density falloff for both cases over the first two cm from the source plane. When elastic collisions were absent the density fell off faster in deeper zones. Note that this is the same behavior, as seen in the highest density region of Fig. 7. When elastic collisions are absent the neutral atoms travel much farther in the perpendicular direction along the plate, contributing less directed flux capable of penetrating along the field lines into the densest plasma.

Figure 8(b) shows the average energy of the neutral atoms as a function of distance from the divertor plate. The DEGAS code gives a Frank–Condon energy of 4 eV to a neutral atom from a dissociation. Reflected atoms will have more energy and are therefore less likely to be present in the first zone. Energy can also be gained through charge exchange. The deepest neutrals are the coolest in the case of elastic collisions because the elastic scattering events take away energy. Those neutrals at 3 cm from the plate have had more elastic collisions on average then the ones at 1.5 cm from the plate. When elastic collisions are not included the energy is much more constant, as a function of penetration depth.

C. Transmittance through a pump duct and gaseous divertor

Another topic of interest is the transmittance of neutral atoms through a gas-filled volume. If neutral–molecule elastic collisions are not taken into account, the atoms will go in straight lines until they strike a wall. As the size of fusion devices increase, the mean-free path for elastic scattering becomes much less than the radial dimensions of the pipe. To simulate these effects on pumping, a pump duct 700 cm long and 120 cm wide was simulated with neutral atoms sourced from one end. The neutral molecular density was held constant in the entire duct at 3×10^{13} cm^{-3}. (1 mTorr). For 1000 particle flights sourced 5430 neutral atom–molecule collisions occurred.

Figure 9 shows the density distribution as a function of distance from the source. When no elastic collisions were included the density fell off exponentially, as collisions with the walls eventually turned the atoms into molecules. The flux of atoms to the walls fell gradually by one order of magnitude over the first 300 cm, and stayed at that level to the end. Of course, those atoms that were heading straight down the pipe made it to the end and the flux of atoms at the end of the duct was approximately one-third of the flux to the front edges of the tube. When elastic collisions were included, no atoms made it to the end of the duct. The flux distribution on the walls again fell by one order of magnitude after 300 cm, but fell by two orders of magnitude after

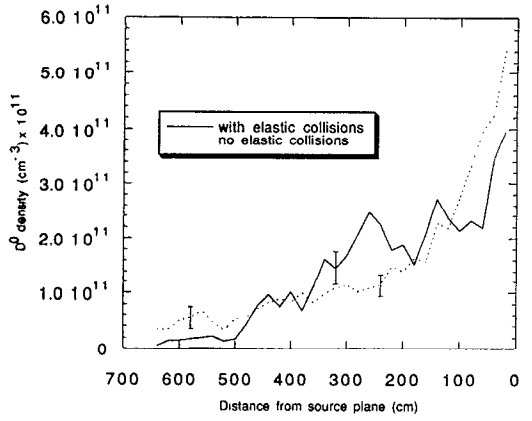

FIG. 9. Transmittance of neutral atoms down a pump duct with 1 mTorr of H_2. The average density across the 120 cm duct as a function of distance from the source is shown with and without including elastic collisions. The statistical error in the data is on the order of the fluctuations seen in the data. Representative error bars are shown.

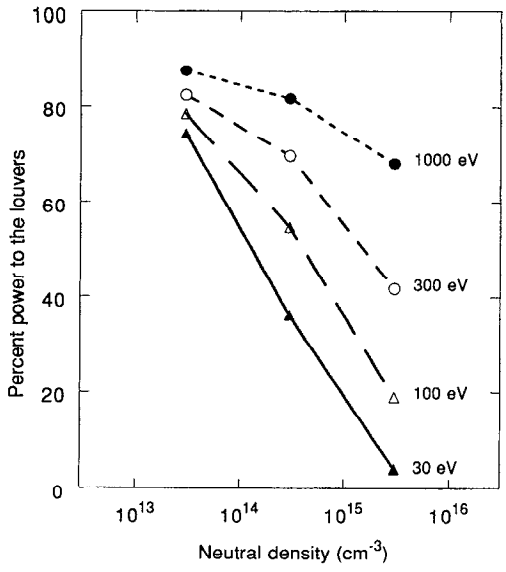

FIG. 10. Percent of energy transfered to the louvers placed in a gaseous divertor as a function of the incident atom energy. As the neutral density is increased more energy is transferred by elastic scattering to the neutral background gas. This effect is greatest for lower-energy incident atoms. If no elastic scattering were included, 100% of the power would be transfered to the louvers. The statistical error in this data is less than 5%. Error bars are on the order of the size of the data points.

500 cm. Including elastic collisions, the density of the neutral atoms falls linearly with distance and eventually disappears.

Another example of fast neutral atoms entering a gas-filled volume is a gaseous divertor. Here louvers would be placed relatively close together to try to raise the neutral density and present a large surface area on which to absorb energy.[14] If the effect of elastic collisions is large enough the concept would work and the energy from the incident atoms would be spread over the length of the plates by losing power to the molecules. To simulate this effect two parallel *W* plates, 10 cm apart were modeled. Fast neutral atoms of 30, 100, 300, and 1000 eV entered the simulation at a 45° angle in both the toroidal and poloidal direction at one end of the plates.

Figure 10 shows the percent of power to the louvers as a function of incident energy and neutral molecular density. If no elastic collisions occurred, 100% of the power would be transferred to the louvers from the energetic atoms. As the neutral density is raised from 3×10^{13} cm^{-3} (1 mTorr) to 3×10^{14} cm^{-3} (10 mTorr) and 3×10^{15} cm^{-3} (100 mTorr), the effect of elastic scattering increases and the percent of power to the louvers falls. Due to the higher elastic scattering cross section at lower energy, the lowest-energy atoms are attenuated the most. Enough flights were run to achieve a 5% statistical accuracy in the results.

IV. CONCLUSIONS

The elastic scattering of neutral atoms is the dominant reaction in low-temperature plasmas. Since the transport of neutral atoms is central to the study of edge plasmas and to the design of future magnetic fusion devices, modeling efforts must simulate these reactions. This paper has detailed one method of including neutral atoms elastic scattering into such a code. The effects of including elastic scattering varied the density and flux profiles of neutrals for all three test simulations: transport through a dilute edge plasma, penetration into a dense plasma form the divertor plate, and the transmittance of neutral atoms through a molecular gas of a pump duct or a gaseous divertor.

ACKNOWLEDGMENTS

I would like to thank Dr. David Schultz at the Atomic Data Center, Oak Ridge National Laboratory, for help in finding the interatomic potentials; students Robert Turkot, Jr., Daniel Juliano, and Jeffrey Hasterok for preparation of the figures; and Dr. Samuel A. Cohen at the Princeton Plasma Physics Laboratory for the suggestion to investigate a gaseous divertor.

This work was performed under U.S. Department of Energy Contract No. DEFG02-89-ER52159.

[1] D. B. Heifetz, D. Post, M. Petravic, J. Weisheit, and G. Bateman, J. Comput. Phys. **46**, 309 (1982).
[2] B. H. Bransden and C. J. Joachain, *Physics of Atoms and Molecules* (Longman, London, 1983).
[3] A. J. C. Varandas, J. Chem. Phys. **70**, 3786 (1979).
[4] A. J. C. Varandas and J. Tennyson, Chem. Phys. Lett. **77**, 151 (1981).
[5] K. T. Tang and J. P. Toennies, Chem. Phys. Lett. **151**, 301 (1988).
[6] A. Russek and R. Garcia, Phys. Rev. A **26**, 1924 (1982).
[7] J. Jakacky, Jr., E. Pollack, R. Snyder, and A. Russek, Phys. Rev. A **31**, 2149 (1985).
[8] A. M. Myers, Ph.D. dissertation, University of Illinois, 1991.
[9] A. A. Abrahamson, Phys. Rev. **76**, 178 (1969).
[10] E. J. Purcell, *Calculus with Analytic Geometry*, 3rd ed. (Prentice–Hall, Englewood Cliffs, NJ, 1978).
[11] W. H. Press, B. P. Flannery, S. A. Teukolsky, and W. T. Vetterling, in *Integration of Functions* (Cambridge University Press, New York, 1986), Chap. 4.
[12] D. Reiter (personal communication, 1992).
[13] B. Braams, in *Europhysics Conference Abstracts*, 9f (European Physical Society, Geneva, 1985), p. 480.
[14] S. A. Cohen (personal communication, November 1992).